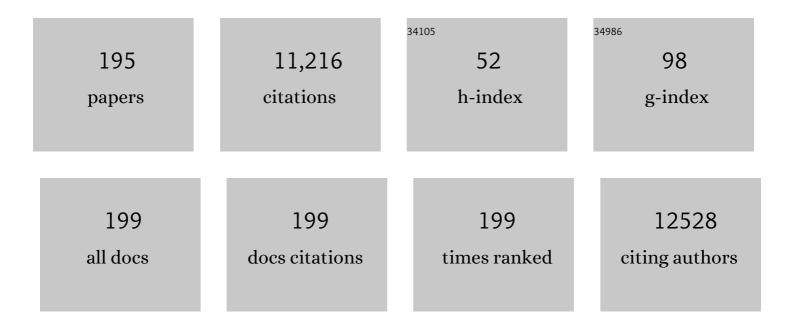
List of Publications by Year in descending order

Source: https://exaly.com/author-pdf/1858947/publications.pdf Version: 2024-02-01



Ілм 7ні Нії

#	Article	IF	CITATIONS
1	Coordinatively Unsaturated Al ³⁺ Centers as Binding Sites for Active Catalyst Phases of Platinum on γ-Al ₂ O ₃ . Science, 2009, 325, 1670-1673.	12.6	790
2	A Stable Vanadium Redoxâ€Flow Battery with High Energy Density for Largeâ€Scale Energy Storage. Advanced Energy Materials, 2011, 1, 394-400.	19.5	688
3	Materials Science and Materials Chemistry for Large Scale Electrochemical Energy Storage: From Transportation to Electrical Grid. Advanced Functional Materials, 2013, 23, 929-946.	14.9	590
4	Anodeâ€Free Rechargeable Lithium Metal Batteries. Advanced Functional Materials, 2016, 26, 7094-7102.	14.9	495
5	Lactic Acid Is Elevated in Idiopathic Pulmonary Fibrosis and Induces Myofibroblast Differentiation via pH-Dependent Activation of Transforming Growth Factor-β. American Journal of Respiratory and Critical Care Medicine, 2012, 186, 740-751.	5.6	265
6	Quantitatively Probing the Al Distribution in Zeolites. Journal of the American Chemical Society, 2014, 136, 8296-8306.	13.7	199
7	Investigation of the rechargeability of Li–O2 batteries in non-aqueous electrolyte. Journal of Power Sources, 2011, 196, 5674-5678.	7.8	197
8	The stability of organic solvents and carbon electrode in nonaqueous Li-O2 batteries. Journal of Power Sources, 2012, 215, 240-247.	7.8	197
9	A facile approach using MgCl2 to formulate high performance Mg2+ electrolytes for rechargeable Mg batteries. Journal of Materials Chemistry A, 2014, 2, 3430.	10.3	197
10	Towards understanding the poor thermal stability of V5+ electrolyte solution in Vanadium Redox Flow Batteries. Journal of Power Sources, 2011, 196, 3669-3672.	7.8	194
11	Towards Highâ€Performance Nonaqueous Redox Flow Electrolyte Via Ionic Modification of Active Species. Advanced Energy Materials, 2015, 5, 1400678.	19.5	181
12	Penta-coordinated Al3+ ions as preferential nucleation sites for BaO on γ-Al2O3: An ultra-high-magnetic field 27Al MAS NMR study. Journal of Catalysis, 2007, 251, 189-194.	6.2	173
13	Carbon-13 chemical shift anisotropies of solid amino acids. Magnetic Resonance in Chemistry, 1993, 31, 699-704.	1.9	146
14	A sensitive, high resolution magic angle turning experiment for measuring chemical shift tensor principal values. Molecular Physics, 1998, 95, 1113-1126.	1.7	138
15	Direct Observation of the Active Center for Methane Dehydroaromatization Using an Ultrahigh Field ⁹⁵ Mo NMR Spectroscopy. Journal of the American Chemical Society, 2008, 130, 3722-3723.	13.7	134
16	Magic-Angle-Turning Experiments for Measuring Chemical-Shift-Tensor Principal Values in Powdered Solids. Journal of Magnetic Resonance Series A, 1995, 113, 210-222.	1.6	133
17	Synthesis, characterization, and catalytic function of novel highly dispersed tungsten oxide catalysts on mesoporous silica. Journal of Catalysis, 2006, 239, 200-211.	6.2	130
18	Chloride supporting electrolytes for all-vanadium redox flow batteries. Physical Chemistry Chemical Physics, 2011, 13, 18186.	2.8	126

#	Article	IF	CITATIONS
19	Reduction Mechanism of Fluoroethylene Carbonate for Stable Solid–Electrolyte Interphase Film on Silicon Anode. ChemSusChem, 2014, 7, 549-554.	6.8	126
20	Improving Lithium–Sulfur Battery Performance under Lean Electrolyte through Nanoscale Confinement in Soft Swellable Gels. Nano Letters, 2017, 17, 3061-3067.	9.1	122
21	Nanocomposite polymer electrolyte for rechargeable magnesium batteries. Nano Energy, 2015, 12, 750-759.	16.0	121
22	Genesis and Stability of Hydronium Ions in Zeolite Channels. Journal of the American Chemical Society, 2019, 141, 3444-3455.	13.7	119
23	<i>In Situ</i> Molecular Spectroscopic Evidence for CO ₂ Intercalation into Montmorillonite in Supercritical Carbon Dioxide. Langmuir, 2012, 28, 7125-7128.	3.5	117
24	Combined ^{6,7} Li NMR and Molecular Dynamics Study of Li Diffusion in Li ₂ TiO ₃ . Journal of Physical Chemistry C, 2009, 113, 20108-20116.	3.1	107
25	Spectroscopic investigations of the fouling process on Nafion membranes in vanadium redox flow batteries. Journal of Membrane Science, 2011, 366, 325-334.	8.2	107
26	Following the Transient Reactions in Lithium–Sulfur Batteries Using an In Situ Nuclear Magnetic Resonance Technique. Nano Letters, 2015, 15, 3309-3316.	9.1	107
27	Role of Pentacoordinated Al ³⁺ Ions in the High Temperature Phase Transformation of γ-Al ₂ O ₃ . Journal of Physical Chemistry C, 2008, 112, 9486-9492.	3.1	106
28	Production of Diethyl Carbonate from Ethanol and Carbon Monoxide over a Heterogeneous Catalyst. Energy & Fuels, 2002, 16, 177-181.	5.1	104
29	The role of H2O in the carbonation of forsterite in supercritical CO2. International Journal of Greenhouse Gas Control, 2011, 5, 1081-1092.	4.6	103
30	Unique Role of Anchoring Penta-Coordinated Al ³⁺ Sites in the Sintering of γ-Al ₂ O ₃ -Supported Pt Catalysts. Journal of Physical Chemistry Letters, 2010, 1, 2688-2691.	4.6	101
31	Reaction of water-saturated supercritical CO2 with forsterite: Evidence for magnesite formation at low temperatures. Geochimica Et Cosmochimica Acta, 2012, 91, 271-282.	3.9	97
32	Mechanism by which Tungsten Oxide Promotes the Activity of Supported V ₂ O ₅ /TiO ₂ Catalysts for NO _{<i>X</i>} Abatement: Structural Effects Revealed by ⁵¹ V MAS NMR Spectroscopy. Angewandte Chemie - International Edition, 2019, 58, 12609-12616.	13.8	96
33	An Isotropic Chemical Shift-Chemical Shift Anisotropy Magic-Angle Slow-Spinning 2D NMR Experiment. Journal of Magnetic Resonance Series A, 1993, 105, 82-87.	1.6	94
34	Metal Carbonation of Forsterite in Supercritical CO ₂ and H ₂ O Using Solid State ²⁹ Si, ¹³ C NMR Spectroscopy. Journal of Physical Chemistry C, 2010, 114, 4126-4134.	3.1	89
35	Elucidating the higher stability of vanadium(V) cations in mixed acid based redox flow battery electrolytes. Journal of Power Sources, 2013, 241, 173-177.	7.8	85
36	Solvent-determined mechanistic pathways in zeolite-H-BEA-catalysed phenol alkylation. Nature Catalysis, 2018, 1, 141-147.	34.4	85

#	Article	IF	CITATIONS
37	Nuclear magnetic resonance studies on vanadium(IV) electrolyte solutions for vanadium redox flow battery. Journal of Power Sources, 2010, 195, 7709-7717.	7.8	84
38	15N Chemical Shift Tensors in Nucleic Acid Bases. Journal of the American Chemical Society, 1998, 120, 9863-9869.	13.7	80
39	Insights into silicate carbonation processes in water-bearing supercritical CO2 fluids. International Journal of Greenhouse Gas Control, 2013, 15, 104-118.	4.6	80
40	Boehmite and Gibbsite Nanoplates for the Synthesis of Advanced Alumina Products. ACS Applied Nano Materials, 2018, 1, 7115-7128.	5.0	79
41	Polymer-Ceramic Conversion of Liquid Polyaluminasilazanes for SiAlCN Ceramics. Journal of the American Ceramic Society, 2005, 88, 2415-2419.	3.8	69
42	Solvent Evaporation Assisted Preparation of Oriented Nanocrystalline Mesoporous MFI Zeolites. ACS Catalysis, 2011, 1, 682-690.	11.2	67
43	Lithium diffusion in Li4Ti5O12 at high temperatures. Journal of Power Sources, 2011, 196, 2211-2220.	7.8	65
44	Structural Determination in Carbonaceous Solids Using Advanced Solid State NMR Techniques. Energy & Fuels, 2001, 15, 14-22.	5.1	64
45	Investigation of Aluminum Site Changes of Dehydrated Zeolite H-Beta during a Rehydration Process by High-Field Solid-State NMR. Journal of Physical Chemistry C, 2015, 119, 1410-1417.	3.1	63
46	High-resolution1H NMR spectroscopy in organs and tissues using slow magic angle spinning. Magnetic Resonance in Medicine, 2001, 46, 213-218.	3.0	61
47	Investigation of local environments in Nafion–SiO2 composite membranes used in vanadium redox flow batteries. Solid State Nuclear Magnetic Resonance, 2012, 42, 71-80.	2.3	61
48	Effect of Chemical Lithium Insertion into Rutile TiO ₂ Nanorods. Journal of Physical Chemistry C, 2009, 113, 14567-14574.	3.1	59
49	Natural abundance 17O, 6Li NMR and molecular modeling studies of the solvation structures of lithium bis(fluorosulfonyl)imide/1,2-dimethoxyethane liquid electrolytes. Journal of Power Sources, 2016, 307, 231-243.	7.8	58
50	Metabolomics in Lung Inflammation:A High-Resolution ¹ H NMR Study of Mice Exposedto Silica Dust. Toxicology Mechanisms and Methods, 2008, 18, 385-398.	2.7	57
51	Following Solidâ€Acidâ€Catalyzed Reactions by MAS NMR Spectroscopy in Liquid Phase—Zeoliteâ€Catalyzed Conversion of Cyclohexanol in Water. Angewandte Chemie - International Edition, 2014, 53, 479-482.	13.8	57
52	Probing Lithium Germanide Phase Evolution and Structural Change in a Germanium-in-Carbon Nanotube Energy Storage System. Journal of the American Chemical Society, 2015, 137, 2600-2607.	13.7	57
53	Mechanism of Phenol Alkylation in Zeolite H-BEA Using In Situ Solid-State NMR Spectroscopy. Journal of the American Chemical Society, 2017, 139, 9178-9185.	13.7	56
54	The superior hydrothermal stability of Pd/SSZ-39 in low temperature passive NOx adsorption (PNA) and methane combustion. Applied Catalysis B: Environmental, 2021, 280, 119449.	20.2	56

#	Article	IF	CITATIONS
55	Structure and stability of hexa-aqua V(iii) cations in vanadium redox flow battery electrolytes. Physical Chemistry Chemical Physics, 2012, 14, 10233.	2.8	55
56	Stability of Zeolites in Aqueous Phase Reactions. Chemistry of Materials, 2017, 29, 7255-7262.	6.7	55
57	A fundamental study on the [(μ-Cl) ₃ Mg ₂ (THF) ₆] ⁺ dimer electrolytes for rechargeable Mg batteries. Chemical Communications, 2015, 51, 2312-2315.	4.1	53
58	<i>In Situ</i> Raman and Nuclear Magnetic Resonance Study of Trapped Lithium in the Solid Electrolyte Interface of Reduced Graphene Oxide. Journal of Physical Chemistry C, 2016, 120, 2600-2608.	3.1	53
59	Investigation of the Structure and Active Sites of TiO ₂ Nanorod Supported VO _{<i>x</i>} Catalysts by High-Field and Fast-Spinning ⁵¹ V MAS NMR. ACS Catalysis, 2015, 5, 3945-3952.	11.2	51
60	Unraveling the Origin of Structural Disorder in High Temperature Transition Al ₂ O ₃ : Structure of Î,-Al ₂ O ₃ . Chemistry of Materials, 2015, 27, 7042-7049.	6.7	51
61	Measurement of 13C chemical shift tensor principal values with a magic-angle turning experiment. Solid State Nuclear Magnetic Resonance, 1994, 3, 181-197.	2.3	50
62	Stereochemical Analysis by Solid-State NMR:Â Structural Predictions in Ambuic Acid. Journal of Organic Chemistry, 2003, 68, 4609-4614.	3.2	50
63	Impact of Aqueous Medium on Zeolite Framework Integrity. Chemistry of Materials, 2015, 27, 3533-3545.	6.7	50
64	Technique for Importing Greater Evolution Resolution in Multidimensional NMR Spectrum. Journal of Magnetic Resonance, 1997, 129, 134-144.	2.1	48
65	High-resolution1H NMR spectroscopy in rat liver using magic angle turning at a 1 Hz spinning rate. Magnetic Resonance in Medicine, 2002, 47, 829-836.	3.0	48
66	Variable Temperature and Pressure Operando MAS NMR for Catalysis Science and Related Materials. Accounts of Chemical Research, 2020, 53, 611-619.	15.6	48
67	High field 27Al MAS NMR and TPD studies of active sites in ethanol dehydration using thermally treated transitional aluminas as catalysts. Journal of Catalysis, 2016, 336, 85-93.	6.2	47
68	Multinuclear NMR Study of the Solid Electrolyte Interface Formed in Lithium Metal Batteries. ACS Applied Materials & Interfaces, 2017, 9, 14741-14748.	8.0	47
69	Hydrolysis of zeolite framework aluminum and its impact on acid catalyzed alkane reactions. Journal of Catalysis, 2018, 365, 359-366.	6.2	47
70	In vivo and ex vivo high-resolution 1H NMR in biological systems using low-speed magic angle spinning. Progress in Nuclear Magnetic Resonance Spectroscopy, 2006, 49, 207-259.	7.5	46
71	Sealed rotors for in situ high temperature high pressure MAS NMR. Chemical Communications, 2015, 51, 13458-13461.	4.1	46
72	Mechanism by which Tungsten Oxide Promotes the Activity of Supported V ₂ O ₅ /TiO ₂ Catalysts for NO _{<i>X</i>} Abatement: Structural Effects Revealed by ⁵¹ V MAS NMR Spectroscopy. Angewandte Chemie, 2019, 131, 12739-12746.	2.0	45

#	Article	IF	CITATIONS
73	Synthesis of nanodispersed oxides of vanadium, titanium, molybdenum, and tungsten on mesoporous silica using atomic layer deposition. Topics in Catalysis, 2006, 39, 245-255.	2.8	43
74	Solid-State Hydriding Mechanism in the LiBH ₄ + MgH ₂ System. Journal of Physical Chemistry C, 2010, 114, 8089-8098.	3.1	43
75	Characterization of Dispersed Heteropoly Acid on Mesoporous Zeolite Using Solid-State ³¹ P NMR Spinâ^'Lattice Relaxation. Journal of the American Chemical Society, 2009, 131, 9715-9721.	13.7	42
76	High-pressure magic angle spinning nuclear magnetic resonance. Journal of Magnetic Resonance, 2011, 212, 378-385.	2.1	42
77	Elucidating graphene–ionic liquid interfacial region: A combined experimental and computational study. Nano Energy, 2014, 3, 152-158.	16.0	42
78	High-resolution1H NMR spectroscopy in a live mouse subjected to 1.5 Hz magic angle spinning. Magnetic Resonance in Medicine, 2003, 50, 1113-1119.	3.0	41
79	A new class of highly dispersed VOx catalysts on mesoporous silica: Synthesis, characterization, and catalytic activity in the partial oxidation of ethanol. Applied Catalysis A: General, 2006, 300, 109-119.	4.3	41
80	Transitions in Al Coordination during Gibbsite Crystallization Using High-Field ²⁷ Al and ²³ Na MAS NMR Spectroscopy. Journal of Physical Chemistry C, 2017, 121, 27555-27562.	3.1	41
81	Studies of Secondary Melanoma on C57BL/6J Mouse Liver Using 1H NMR Metabolomics. Metabolites, 2013, 3, 1011-1035.	2.9	40
82	Promotion of protolytic pentane conversion on H-MFI zeolite by proximity of extra-framework aluminum oxide and BrA,nsted acid sites. Journal of Catalysis, 2019, 370, 424-433.	6.2	40
83	Clay Hydration/dehydration in Dry to Water-saturated Supercritical CO2: Implications for Caprock Integrity. Energy Procedia, 2013, 37, 5443-5448.	1.8	39
84	Investigation of Silica-Supported Vanadium Oxide Catalysts by High-Field ⁵¹ V Magic-Angle Spinning NMR. Journal of Physical Chemistry C, 2017, 121, 6246-6254.	3.1	39
85	Palladium/Zeolite Low Temperature Passive NOx Adsorbers (PNA): Structure-Adsorption Property Relationships for Hydrothermally Aged PNA Materials. Emission Control Science and Technology, 2020, 6, 126-138.	1.5	38
86	²⁷ Al MAS NMR Studies of HBEA Zeolite at Low to High Magnetic Fields. Journal of Physical Chemistry C, 2017, 121, 12849-12854.	3.1	37
87	25Mg NMR and computational modeling studies of the solvation structures and molecular dynamics in magnesium based liquid electrolytes. Nano Energy, 2018, 46, 436-446.	16.0	37
88	Formation of submicron magnesite during reaction of natural forsterite in H2O-saturated supercritical CO2. Geochimica Et Cosmochimica Acta, 2014, 134, 197-209.	3.9	36
89	Sensitivity-enhanced phase-corrected ultra-slow magic angle turning using multiple-echo data acquisition. Journal of Magnetic Resonance, 2003, 163, 149-162.	2.1	35
90	<i>In situ</i> and <i>ex situ</i> NMR for battery research. Journal of Physics Condensed Matter, 2018, 30, 463001.	1.8	35

#	Article	IF	CITATIONS
91	Single-Step Conversion of Ethanol to <i>n</i> Butene over Ag-ZrO ₂ /SiO ₂ Catalysts. ACS Catalysis, 2020, 10, 10602-10613.	11.2	34
92	Rotor design for high pressure magic angle spinning nuclear magnetic resonance. Journal of Magnetic Resonance, 2013, 226, 64-69.	2.1	33
93	In Situ ²⁷ Al NMR Spectroscopy of Aluminate in Sodium Hydroxide Solutions above and below Saturation with Respect to Gibbsite. Inorganic Chemistry, 2018, 57, 11864-11873.	4.0	33
94	Line narrowing in 1H MAS spectrum of mesoporous silica by removing adsorbed H2O using N2. Solid State Nuclear Magnetic Resonance, 2005, 27, 200-205.	2.3	32
95	Understanding Aqueous Electrolyte Stability through Combined Computational and Magnetic Resonance Spectroscopy: A Case Study on Vanadium Redox Flow Battery Electrolytes. ChemPlusChem, 2015, 80, 428-437.	2.8	32
96	Low temperature milling of the LiNH2 + LiH hydrogen storage system. International Journal of Hydrogen Energy, 2009, 34, 4331-4339.	7.1	29
97	Studies of the Active Sites for Methane Dehydroaromatization Using Ultrahigh-Field Solid-State 95Mo NMR Spectroscopy. Journal of Physical Chemistry C, 2009, 113, 2936-2942.	3.1	29
98	Natural abundance 17O nuclear magnetic resonance and computational modeling studies of lithium based liquid electrolytes. Journal of Power Sources, 2015, 285, 146-155.	7.8	29
99	Elementary Steps of Faujasite Formation Followed by in Situ Spectroscopy. Chemistry of Materials, 2018, 30, 888-897.	6.7	29
100	Unraveling Gibbsite Transformation Pathways into LiAl-LDH in Concentrated Lithium Hydroxide. Inorganic Chemistry, 2019, 58, 12385-12394.	4.0	29
101	High-Field One-Dimensional and Two-Dimensional ²⁷ Al Magic-Angle Spinning Nuclear Magnetic Resonance Study of Î,-, δ-, and γ-Al ₂ O ₃ Dominated Aluminum Oxides: Toward Understanding the Al Sites in γ-Al ₂ O ₃ . ACS Omega, 2021, 6, 4090-4099.	3.5	29
102	Modified Spectral Editing Methods for 13C CP/MAS Experiments in Solids. Journal of Magnetic Resonance, 2000, 142, 326-330.	2.1	27
103	Dynamic High-Resolution1H and31P NMR Spectroscopy and1H T2Measurements in Postmortem Rabbit Muscles Using Slow Magic Angle Spinning. Journal of Agricultural and Food Chemistry, 2004, 52, 2681-2688.	5.2	27
104	Dynamic Structural Changes of SiO ₂ Supported Pt–Ni Bimetallic Catalysts over Redox Treatments Revealed by NMR and EPR. Journal of Physical Chemistry C, 2015, 119, 21219-21226.	3.1	27
105	Role of Solvent Rearrangement on Mg ²⁺ Solvation Structures in Dimethoxyethane Solutions using Multimodal NMR Analysis. Journal of Physical Chemistry Letters, 2020, 11, 6443-6449.	4.6	27
106	Solid State NMR and Wide Angle X-ray Diffraction Studies of Supercritical Fluid CO2-Treated Poly(ethylene terephthalate). Macromolecules, 1998, 31, 9238-9246.	4.8	26
107	Study the effects of mechanical activation on Li–N–H systems with 1H and 6Li solid-state NMR. Journal of Power Sources, 2007, 170, 419-424.	7.8	26
108	Investigating the Surface Structure of γ-Al ₂ O ₃ Supported WO _X Catalysts by High Field ²⁷ Al MAS NMR and Electronic Structure Calculations. Journal of Physical Chemistry C, 2016, 120, 23093-23103.	3.1	26

#	Article	IF	CITATIONS
109	Origin of Unusual Acidity and Li ⁺ Diffusivity in a Series of Water-in-Salt Electrolytes. Journal of Physical Chemistry B, 2020, 124, 5284-5291.	2.6	26
110	Localized in vivo isotropic-anisotropic correlation1H NMR spectroscopy using ultraslow magic angle spinning. Magnetic Resonance in Medicine, 2006, 55, 41-49.	3.0	25
111	Probing the reaction pathway of dehydrogenation of the LiNH2+LiH mixture using in situ 1H NMR spectroscopy. Journal of Power Sources, 2008, 181, 116-119.	7.8	25
112	Hydrogen Bonding Effects on the13C NMR Chemical Shift Tensors of Some Amino Acids in the Solid State. Magnetic Resonance in Chemistry, 1997, 35, 606-608.	1.9	24
113	Effects of Novel Supports on the Physical and Catalytic Properties of Tungstophosphoric Acid for Alcohol Dehydration Reactions. Topics in Catalysis, 2008, 49, 259-267.	2.8	24
114	Diffusional motion of redox centers in carbonate electrolytes. Journal of Chemical Physics, 2014, 141, 104509.	3.0	24
115	<i>In Situ</i> High Temperature High Pressure MAS NMR Study on the Crystallization of AIPO ₄ -5. Journal of Physical Chemistry C, 2016, 120, 1701-1708.	3.1	23
116	Direct observation of ion exchange in mechanically activated LiH+MgB2 system using ultrahigh field nuclear magnetic resonance spectroscopy. Applied Physics Letters, 2009, 94, 141905.	3.3	22
117	Highly Dispersed and Active ReO _{<i>x</i>} on Alumina-Modified SBA-15 Silica for 2-Butanol Dehydration. ACS Catalysis, 2012, 2, 1020-1026.	11.2	22
118	The evaluation of different MAS techniques at low spinning rates in aqueous samples and in the presence of magnetic susceptibility gradients. Journal of Magnetic Resonance, 2002, 159, 92-100.	2.1	21
119	Conversion of ethanol to 1,3–butadiene over Ag–ZrO2/SiO2 catalysts: The role of surface interfaces. Journal of Energy Chemistry, 2021, 54, 7-15.	12.9	21
120	Activity of Cu–Al–Oxo Extra-Framework Clusters for Selective Methane Oxidation on Cu-Exchanged Zeolites. Jacs Au, 2021, 1, 1412-1421.	7.9	21
121	A large sample volume magic angle spinning nuclear magnetic resonance probe for in situ investigations with constant flow of reactants. Physical Chemistry Chemical Physics, 2012, 14, 2137-2143.	2.8	20
122	In situ 7Li and 133Cs nuclear magnetic resonance investigations on the role of Cs+ additive in lithium-metal deposition process. Journal of Power Sources, 2016, 304, 51-59.	7.8	20
123	WO supported on γ-Al2O3 with different morphologies as model catalysts for alkanol dehydration. Journal of Catalysis, 2018, 363, 1-8.	6.2	20
124	Catalytic activation of ethylene C–H bonds on uniform d ⁸ Ir(<scp>i</scp>) and Ni(<scp>ii</scp>) cations in zeolites: toward molecular level understanding of ethylene polymerization on heterogeneous catalysts. Catalysis Science and Technology, 2019, 9, 6570-6576.	4.1	20
125	Structure–Activity Relationships of Hydrothermally Aged Titania-Supported Vanadium–Tungsten Oxide Catalysts for SCR of NO _{<i>x</i>} Emissions with NH ₃ . ACS Catalysis, 2021, 11, 12096-12111.	11.2	20
126	Pulsed Field Gradient Nuclear Magnetic Resonance and Diffusion Analysis in Battery Research. Chemistry of Materials, 2021, 33, 8562-8590.	6.7	20

#	Article	IF	CITATIONS
127	Multiphase sequestration geochemistry: Model for mineral carbonation. Energy Procedia, 2011, 4, 5009-5016.	1.8	19
128	Transformation of Gibbsite to Boehmite in Caustic Aqueous Solution at Hydrothermal Conditions. Crystal Growth and Design, 2019, 19, 5557-5567.	3.0	19
129	Adsorption and Thermal Decomposition of Electrolytes on Nanometer Magnesium Oxide: An in Situ 13C MAS NMR Study. ACS Applied Materials & Interfaces, 2019, 11, 38689-38696.	8.0	19
130	Ab initio calculation and experimental determination of the 13C chemical shielding tensors of 4,4′-dimethoxybiphenyl. Computational and Theoretical Chemistry, 1998, 428, 283-286.	1.5	18
131	Investigation of mechanical activation on Li–N–H systems using 6Li magic angle spinning nuclear magnetic resonance at ultra-high field. Journal of Power Sources, 2008, 182, 278-283.	7.8	18
132	1H NMR metabolomics study of metastatic melanoma in C57BL/6J mouse spleen. Metabolomics, 2014, 10, 1129-1144.	3.0	18
133	Preferential Solvation of an Asymmetric Redox Molecule. Journal of Physical Chemistry C, 2016, 120, 27834-27839.	3.1	18
134	NMR-based Metabolomics Analysis of Liver from C57BL/6 Mouse Exposed to Ionizing Radiation. Radiation Research, 2017, 188, 44.	1.5	17
135	Factors Influencing Preferential Anion Interactions during Solvation of Multivalent Cations in Ethereal Solvents. Journal of Physical Chemistry C, 2021, 125, 6005-6012.	3.1	17
136	Dynamic nuclear polarization of nitrogen-15 in benzamide. Solid State Nuclear Magnetic Resonance, 1997, 8, 129-137.	2.3	16
137	H and 15N Dynamic Nuclear Polarization Studies of Carbazole. Journal of Physical Chemistry A, 2000, 104, 4413-4420.	2.5	16
138	Ring-chain tautomerism in solid-phase erythromycin A: evidence by solid-state NMR. Solid State Nuclear Magnetic Resonance, 2003, 24, 23-38.	2.3	16
139	Detailed investigation of ion exchange in ball-milled LiH+MgB2 system using ultra-high field nuclear magnetic resonance spectroscopy. Journal of Power Sources, 2010, 195, 3645-3648.	7.8	16
140	The use of differential transverse relaxation to detect mobile species in solids. Solid State Nuclear Magnetic Resonance, 1996, 6, 63-71.	2.3	15
141	Quantum chemical calculation and experimental measurement of the 13C chemical shift tensors of vanillin and 3,4-dimethoxybenzaldehyde. Chemical Physics Letters, 1997, 266, 533-536.	2.6	15
142	Nuclear magnetic resonance studies of the solvation structures of a high-performance nonaqueous redox flow electrolyte. Journal of Power Sources, 2016, 308, 172-179.	7.8	15
143	²⁷ Al Pulsed Field Gradient, Diffusion–NMR Spectroscopy of Solvation Dynamics and Ion Pairing in Alkaline Aluminate Solutions. Journal of Physical Chemistry B, 2018, 122, 10907-10912.	2.6	15
144	Solid-state hydrogen storage: Storage capacity, thermodynamics, and kinetics. Jom, 2009, 61, 45-51.	1.9	14

#	Article	IF	CITATIONS
145	Application of High-Resolution ¹ H MAS NMR Spectroscopy to the Analysis of Intact Bones from Mice Exposed to Gamma Radiation. Radiation Research, 2009, 172, 607-616.	1.5	14
146	Low-temperature (< 200°C) degradation of electronic nicotine delivery system liquids generates toxic aldehydes. Scientific Reports, 2021, 11, 7800.	3.3	14
147	Solid-State 13C NMR, X-ray, and Quantum Mechanical Studies of the Carbon Chemical Shifts Tensors of p-Tolyl Ether. The Journal of Physical Chemistry, 1994, 98, 12186-12190.	2.9	13
148	High resolution 1H spectra of powdered solids observed by Hahn echo pulse sequence with magic-angle spinning. Solid State Nuclear Magnetic Resonance, 1996, 6, 85-94.	2.3	13
149	Investigation of water assisted phase transformation process from AIPO4-5 to AIPO4-tridymite. Microporous and Mesoporous Materials, 2016, 223, 241-246.	4.4	13
150	Probing Conformational Evolution and Associated Dynamics of Mg(N(SO ₂ CF ₃) ₂) ₂ A·Dimethoxyethane Adduct Using Solid-State ¹⁹ F and ¹ H NMR. Journal of Physical Chemistry C, 2020, 124, 4999-5008.	3.1	13
151	A High-Resolution 3D Separated-Local-Field Experiment by Means of Magic-Angle Turning. Journal of Magnetic Resonance, 1997, 126, 120-126.	2.1	12
152	Slow-MAS NMR: A new technology for in vivo metabolomic studies. Drug Discovery Today: Technologies, 2005, 2, 291-294.	4.0	12
153	Spectral editing in 13C CP/MAS experiments at high magnetic field. Solid State Nuclear Magnetic Resonance, 1996, 6, 187-196.	2.3	11
154	Solid-State 13C NMR Measurements in Methoxynaphthalenes:  Determination of the Substituent Chemical Shift Effects in the Principal Values. Journal of Physical Chemistry A, 1997, 101, 9169-9175.	2.5	11
155	Measurement of spin-lattice relaxation times of 13C in organic solids. Solid State Nuclear Magnetic Resonance, 1997, 7, 291-299.	2.3	11
156	Investigation of Polyethylene by Means of Magic Angle Turning and Separated-Local-Field Experiments. Macromolecules, 2000, 33, 3359-3367.	4.8	11
157	Characterizing Surface Acidic Sites in Mesoporous-Silica-Supported Tungsten Oxide Catalysts Using Solid-State NMR and Quantum Chemistry Calculations. Journal of Physical Chemistry C, 2011, 115, 23354-23362.	3.1	11
158	Energetics of Defects on Graphene through Fluorination. ChemSusChem, 2014, 7, 1295-1300.	6.8	10
159	Intermediate Species in the Crystallization of Sodium Aluminate Hydroxy Hydrates. Journal of Physical Chemistry C, 2020, 124, 12337-12345.	3.1	10
160	Investigation of Coal and a Naphthalene Pitch by Means of the Triple-Echo Magic Angle Turning Experiment. Energy & Fuels, 1995, 9, 717-726.	5.1	9
161	Carbon-13 Chemical-Shift Tensors in Polycyclic Aromatic Compounds:  Fluoranthene and Decacyclene. Journal of Physical Chemistry A, 2002, 106, 6477-6482.	2.5	9
162	1H relaxation times of metabolites in biological samples obtained with nondestructiveex-vivo slow-MAS NMR. Magnetic Resonance in Chemistry, 2006, 44, 269-275.	1.9	9

#	Article	IF	CITATIONS
163	Thermal perturbation of NMR properties in small polar and non-polar molecules. Scientific Reports, 2020, 10, 6097.	3.3	9
164	Improvements to the magic angle hopping experiment. Solid State Nuclear Magnetic Resonance, 1993, 2, 235-243.	2.3	8
165	1H Dynamic Nuclear Polarization in Supercritical Ethylene at 1.4 T. Journal of Magnetic Resonance, 2000, 143, 233-239.	2.1	8
166	CP/MAS spectral editing of dried pine leaves. Solid State Nuclear Magnetic Resonance, 1998, 12, 31-36.	2.3	7
167	13C Chemical-shift tensors in an analogous series of heterosubstituted polycyclic aromatic compounds. Magnetic Resonance in Chemistry, 2001, 39, 115-121.	1.9	7
168	Structural analysis of N- and O-glycans using ZIC-HILIC/dialysis coupled to NMR detection. Fungal Genetics and Biology, 2014, 72, 207-215.	2.1	7
169	In Situ Natural Abundance ¹⁷ O and ²⁵ Mg NMR Investigation of Aqueous Mg(OH) ₂ Dissolution in the Presence of Supercritical CO ₂ . Environmental Science & Technology, 2016, 50, 12373-12384.	10.0	7
170	Role of a Multivalent Ion–Solvent Interaction on Restricted Mg ²⁺ Diffusion in Dimethoxyethane Electrolytes. Journal of Physical Chemistry B, 2021, 125, 12574-12583.	2.6	7
171	A simple approach to measuring spin diffusion of abundant nuclei in dipolar-broadened solids. Journal of Magnetic Resonance, 1992, 99, 576-581.	0.5	6
172	A BAYESIAN INTEGRATION MODEL OF HIGH-THROUGHPUT PROTEOMICS AND METABOLOMICS DATA FOR IMPROVED EARLY DETECTION OF MICROBIAL INFECTIONS. , 2008, , .		6
173	Use of relaxation agent doping to shorten very long spin-lattice relaxation times in a magic-angle turning experiment. Solid State Nuclear Magnetic Resonance, 1995, 5, 257-262.	2.3	5
174	A Novel Dipolar Dephasing Method for the Slow Magic Angle Turning Experiment. Journal of Magnetic Resonance, 2001, 152, 7-13.	2.1	5
175	Elucidating the Cooperative Roles of Water and Lewis Acid–Base Pairs in Cascade C–C Coupling and Self-Deoxygenation Reactions. Jacs Au, 2021, 1, 1471-1487.	7.9	5
176	Development and Application of In Situ High-Temperature, High-Pressure Magic Angle Spinning NMR. , 2017, , 1-19.		5
177	High-Temperature and High-Pressure In situ Magic Angle Spinning Nuclear Magnetic Resonance Spectroscopy. Journal of Visualized Experiments, 2020, , .	0.3	5
178	Understanding the Solvation-Dependent Properties of Cyclic Ether Multivalent Electrolytes Using High-Field NMR and Quantum Chemistry. Jacs Au, 2022, 2, 917-932.	7.9	5
179	Investigation of a naphthalene pitch by high-resolution solid-state dynamic nuclear polarization. Solid State Nuclear Magnetic Resonance, 1996, 6, 127-133.	2.3	4
180	Activity of titania and zeolite samples dosed with triethylamine. Microporous and Mesoporous Materials, 2016, 220, 44-57.	4.4	4

#	Article	IF	CITATIONS
181	Sideband separation of protonated and non-protonated carbons in MAS NMR. Chemical Physics Letters, 1992, 195, 159-162.	2.6	3
182	Solid-state NMR studies of 1H spin diffusion in adsorbed organic molecules. Solid State Nuclear Magnetic Resonance, 1993, 2, 97-103.	2.3	3
183	Modeling of the 15N and 13C Chemical Shift Tensors in Purine. ACS Symposium Series, 1999, , 162-176.	0.5	3
184	Magic Angle Spinning NMR Metabolomics. Metabolomics: Open Access, 2016, 6, .	0.1	3
185	Impact of Hydration on Supported V2O5/TiO2 Catalysts as Explored by Magnetic Resonance Spectroscopy. Journal of Physical Chemistry C, 2021, 125, 16766-16775.	3.1	3
186	Slow Magic Angle Sample Spinning: A Non- or Minimally Invasive Method for High-Resolution 1H Nuclear Magnetic Resonance (NMR) Metabolic Profiling. Methods in Molecular Biology, 2011, 708, 335-364.	0.9	3
187	13C high resolution solid state NMR spectra of Chinese coals. Science in China Series D: Earth Sciences, 1997, 40, 65-72.	0.9	2
188	A High-Resolution 13C 3D CSA-CSA-CSA Correlation Experiment by Means of Magic Angle Turning. Journal of Magnetic Resonance, 2000, 145, 230-236.	2.1	2
189	An isotropic chemical shift–chemical shift anisotropic correlation experiment using discrete magic angle turning. Journal of Magnetic Resonance, 2009, 198, 105-110.	2.1	2
190	Innenrücktitelbild: Mechanism by which Tungsten Oxide Promotes the Activity of Supported V ₂ O ₅ /TiO ₂ Catalysts for NO _{<i>X</i>} Abatement: Structural Effects Revealed by ⁵¹ V MAS NMR Spectroscopy (Angew. Chem. 36/2019). Angewandte Chemie, 2019, 131, 12847-12847.	2.0	1
191	Development and Application of In Situ High-Temperature, High-Pressure Magic Angle Spinning NMR. , 2018, , 1073-1091.		1
192	Slow-MAS NMR Methods To Study Metabolic Processes in vivo and in vitro. Special Publication - Royal Society of Chemistry, 0, , 156-165.	0.0	1
193	Modelling complex molecular interactions in catalytic materials for energy storage and conversion in nuclear magnetic resonance. Frontiers in Catalysis, 0, 2, .	3.9	1
194	NMR Metabolomics in Ionizing Radiation. Clinics in Oncology, 2016, 1, .	0.0	0
195	A sensitive, high resolution magic angle turning experiment for measuring chemical shift tensor principal values. Molecular Physics, 1998, 95, 1113-1126.	1.7	О